Heterogeneous Single-Site Catalysts for C–H Activation Reactions: Pd(II)-Loaded S,O-Functionalized Metal Oxide-Bisphosphonates

Niels van Velthoven, Yanhui Wang, Hannah van Hees, Mickaël Henrion, Aram Bugaev, Guillaume Gracy, Kassem Amro, Alexander Soldatov, Johan Alauzun, P. Hubert Mutin, et al.

Heterogeneous Single-Site Catalysts for C-H Activation Reactions: Pd(II)-loaded S,O-Functionalized Metal Oxide-Bisphosphonates

Niels Van Velthoven,[a,†] Yanhui Wang,[b,†] Hannah Van Hees,[a] Mickaël Henrion,[a] Aram L. Bugaev,[c] Guillaume Gracy,[d] Kassem Amro,[d] Alexander V. Soldatov,[c] Johan G. Alauzun,[b] P. Hubert Mutin,[b,*] Dirk E. De Vos[a,*]

a: Centre For Membrane Separations, Adsorption, Catalysis and Spectroscopy for Sustainable Solutions (cMACS), KU Leuven, Celestijnenlaan 200F p. o. box 2461, 3001 Leuven (Belgium).

b: Institut Charles Gerhardt Montpellier, UMR5253 CNRS-UM-ENSCM, Université de Montpellier, 34095 Montpellier (France).

c: The Smart Materials Research Institute, Southern Federal University, Sladkova 178/24, 344090 Rostov-on-Don (Russia).

d: SiKÉMIA, Place Eugène Bataillon, cc1701, 34095 Montpellier (France).

KEYWORDS: *single-site heterogeneous catalyst, oxidative Heck reaction, C-H activation, non-hydrolytic sol-gel, metal oxide-bisphosphonate*

ABSTRACT: Heterogeneous single-site catalysts contain spatially isolated, well-defined active sites. This allows not only their easy recovery by solid-liquid separation, but also the detailed active site design like in homogeneous catalysts. Here, heterogeneous Pd(II) single-site catalysts were assembled, based on mesoporous metal oxide-bisphosphonate materials as supports. This new family of hybrid organic-inorganic materials with tunable porosity was further functionalized with thioether ligands containing S,O-binding sites that enhance the activity of Pd(II) for C-H activation reactions. The structures of the resulting Pd(II) single-site catalysts were carefully analyzed via solid-state NMR spectroscopy, via texture analysis by N_2 physisorption, infrared spectroscopy, and transmission electron microscopy. Furthermore, the immediate environment of the isolated Pd(II) active sites was studied with X-ray absorption spectroscopy. A clear relationship between thioether ligand surface density and catalyst activity could be established. Significantly higher yields were obtained using highly porous metal oxide-bisphosphonate materials as supports compared to materials with lower porosities, such as conventional metal oxides, indicating that the high surface area facilitates the presence of isolated, well-accessible S,O-supported Pd(II) active sites. A wide scope of model substrates, including industrially relevant arenes, can be converted with high yields by the optimal heterogeneous Pd catalyst.

1. INTRODUCTION

Over the past decades, homogeneous catalysis has been increasingly applied for the production of fine chemicals and especially active pharmaceutical ingredients (APIs), ensuring that reactions proceed with high efficiency, high yield, and minimal unwanted by-products.[1,2] However, high costs and price volatility are generally associated with the transition metals that are commonly applied as homogeneous catalysts or catalyst precursors, and traces of noble metals in APIs are strictly regulated.[3,4] Hence, immobilization of the active complex by grafting the ligand on a solid support is an attractive strategy that generates a recyclable heterogeneous catalyst with isolated, well-defined active sites, while potentially preserving the structure-activity relationship of the homogeneous complex.[5–8] As solid support, the use of inorganic materials offers various advantages over organic matrices, such as high chemical, thermal and mechanical stability, and also swelling can largely be avoided.[5] A powerful approach to convert such inorganic metal oxide supports into heterogeneous catalysts with well-defined active sites is by immobilizing molecular complexes on inorganic supports via ligands with silane, carboxylic acid, or phosphonic acid grafting groups.[5,7,8] Nevertheless, reaching similar activities with the immobilized complexes as with the analogous homogeneous catalysts can be particularly difficult.[9,10] Especially for new synthetic strategies that have only been explored fairly recently in homogeneous catalysis, the development of heterogeneous single-site catalysts remains challenging.[11]

Metal-catalyzed coupling reactions via C-H activation have received increased research interest over the past decade as a novel synthesis methodology to couple organic fragments via a C-C bond without the need for prefunctionalization.[12–15] Although many elegant synthesis procedures have already been proposed, they generally rely on substrates bearing directing groups that assist the challenging C-H activation step, which often limits the substrate scope.[16,17] Alternatively, ancillary ligands can be employed to promote the metal-catalyzed cleavage of the C-H bond, even for substrates without directing group.[18] In particular, ligands based on amino acids[19,20], pyridines[21–23], pyridones[24,25], phenanthrolines[26,27], and 4,5-diazafluoren-9-one[28,29] have been reported to increase the reaction rates of various metal-catalyzed undirected C-H activation reactions. Recently, the research teams of Fernández-Ibáñez and Carrow developed a new group of thioether-based ligands.[30–35] These ligands contain a carboxyl group at the α-position of a thioether group and promote the Pd(II)-catalyzed oxidative C-H alkenylation[30,32–35], arylation[31], and acetoxylation[32] of a wide selection of (hetero)arenes. However, even this new generation of Pd catalysts often needs high loadings (5–10

mol %) to reach excellent yields, which hinders their industrial breakthrough.[36] Nevertheless, few heterogeneous catalysts for oxidative C-H alkenylation and arylation reactions have been reported so far,[37,38] of which only a handful are single-site catalysts with well-defined active sites.[39–43] Only very recently, we reported the synthesis of a new family of hybrid organic-inorganic mesoporous materials with tunable porosity and functionality.[44] These bridged metal oxide-bisphosphonates could be promising catalytic supports given their high stability and outstanding textural properties.

Herein, we report the first metal oxide-bisphosphonate-based solid single-site catalyst containing Pd(II)-thioether active sites that greatly accelerate C-H activation.

2. EXPERIMENTAL SECTION

2.1. Synthesis of the Thioether Ligands S1 and S2.

The syntheses of thioether ligands **S1** and **S2** are described in detail in section 1. of the supporting information.

2.2. Synthesis of the Metal Oxide-Bisphosphonate Supports.

2.2.1. TiOP. The titanium oxide-bisphosphonate material was synthesized as described in the literature.[44] Additional samples were prepared by changing the molar ratio of the linker (0.2 eq. of 4,4'-bis(diethylphosphonomethyl)biphenyl (**L1**) instead of 0.1 eq.). All other parameters were kept unchanged.

2.2.2. AlOP. The aluminum oxide oxide-bisphosphonate material was prepared similarly, using 0.63 g (3.08 mmol) aluminum (III) isopropoxide, 0.14 g (0.31 mmol, 0.1 eq.) **L1**, 10 mL toluene, and 0.47 g (0.46 mmol) acetic anhydride.

2.2.3. ZrOP. The zirconium oxide oxide-bisphosphonate material was prepared similarly, using 1.74 g (5.3 mmol) of purified $Zr(O^nPr)_4$ (without 1-propanol), 0.24 g (0.53 mmol, 0.1 eq.) **L1**, and 10 mL 2-pentanone. The synthesis time in the autoclave at 200 °C was extended to 72 h.

2.3. Synthesis of the Metal Oxide Supports

2.3.1. TiO_2. The TiO_2 anatase support was prepared as described in the literature.[45]

2.3.2. Al_2O_3. The amorphous Al_2O_3 support was prepared as described in the literature.[46]

2.3.3. ZrO_2. The ZrO_2 support was obtained via a non-hydrolytic sol-gel procedure. 10 mL 2-pentanone was added to 1.74 g (5.3 mmol) of purified $Zr(O^nPr)_4$ (without 1-propanol). After stirring for 5 min, the resulting solution was transferred to a 23 mL stainless steel autoclave with a PTFE liner. The sealed autoclave was then heated at 240 °C for 72 h in an oven. After the reaction, the gel was thoroughly washed with ether (5 x 30 mL), EtOH (5 x 30 mL), and acetone (5 x 30 mL). Then, it was dried under vacuum (100 Pa) at 120 °C for 5 h. Finally, the material was ground into a fine white powder and was calcined in a muffle furnace at 500 °C (heating rate 10 °C/min) for 5 h in ambient air.

2.4. Grafting of the Thioether Ligand (S1) on the Supports.

2.4.1. TiOP-S1. 0.84 g (3 mmol) thioether ligand (**S1**) was added to 1 g **TiOP** in 30 mL deionized water. The resulting mixture was stirred at 30 °C for 48 h under an inert atmosphere. After the reaction, the precipitate was thoroughly washed with water (10 x 30 mL) and acetone (5 x 30 mL). Finally, it was dried overnight under vacuum (100 Pa) at room temperature and then ground into a fine powder.

2.4.2. AlOP-S1. **S1** was grafted on the aluminum oxide-bisphosphonate support similarly, using 1 g **AlOP**.

2.4.3. ZrOP-S1. **S1** was grafted on the zirconium oxide-bisphosphonate support similarly, using 1 g **ZrOP**.

2.4.4. TiO_2-S1. **S1** was grafted on the zirconium oxide support similarly, using 1 g **TiO_2**.

2.4.5. Al_2O_3-S1. **S1** was grafted on the aluminum oxide support similarly, using 1 g **Al_2O_3**.

2.4.6. ZrO_2-S1. **S1** was grafted on the aluminum oxide support similarly, using 1 g **ZrO_2**.

2.5. Pd-loading of the functionalized supports

The functionalized supports were loaded with typically an equimolar amount of $Pd(OAc)_2$ relative to **S1**. For instance, 14 mg (62.5 µmol) $Pd(OAc)_2$ was added to 190 mg **TiOP-S1** in 3.75 mL dichloromethane at room temperature. After stirring for 24 hours, the solution became transparent and a pale yellow powder was obtained, implying that the Pd(II) centers migrated to the functionalized titanium oxide-bisphosphonate support. After removing the loading solvent under reduced pressure, the active **Pd@TiOP-S1** catalyst was collected and stored under an inert atmosphere.

2.6. Characterization of the Heterogeneous Single-Site Catalysts

A Spectrum II Perkin-Elmer spectrometer was used to collect the Fourier-transform infrared (FTIR) spectra. The structure of the materials was analyzed via scanning electron microscopy (SEM) using a Hitachi S-4800 electron microscope equipped with an Oxford Instruments X-Max ^{N} SDD for energy dispersive X-ray spectroscopy (EDX). The high angle annular dark field scanning transmission electron microscopy (HAADF- STEM) images were measured on a JEOL 2200FS-200 kV microscopy equipped with a JEOL CENTURIO detector for EDX. Nitrogen physisorption was conducted on a Micromeritics 3Flex surface analyzer at 77 K. The specific surface areas were calculated via the multipoint BET)method, the pore size distribution in the 1 to 5 nm range via the DFT method, and in the 2 to 100 nm range via the BJH method applied to the isotherm desorption branch. Solid-state ^{13}C CP-MAS NMR measurements were performed on a 300 MHz VARIAN VNMRS system using a 3.2 mm T3 probe with a sample spinning frequency of 12 kHz. Solid-state ^{31}P MAS NMR spectra were measured on 400 MHz Varian VNMRS spectrometer equipped with a 3.2 mm Varian T3 HXY probe. The spinning frequency was 20 kHz and a 90° excitation pulse with a duration of 3 µs was used in combination with 100 kHz spinal-64 ^1H decoupling. Two hundred scans were recorded with a recycle delay of 30 s. Hydroxyapatite $Ca_{10}(PO_4)_6(OH)_2$ with a signal at 2.8 ppm (relative to 85 wt% H_3PO_4 in water) was used as an external reference to determine the ^{31}P chemical shift accurately. Powder X-ray diffraction (PXRD) data were recorded on a Malvern PANalytical Empyrean diffractometer equipped with at PIXcel 3D 1x1 detector. The patterns were recorded in transmission geometry within a 10° - 70° 2θ-range with a step size of 0.013°. The theoretical patterns

were simulated by Mercury 3.10 based on the corresponding CIF-files. XAS data were collected at the Structural Materials Science beamline of the Kurchatov Synchrotron Radiation Source (Moscow, Russia) in transmission mode for pelletized samples. The energy was selected by a Si(220) channel-cut monochromator. The spectra processing and analysis were conducted using Demeter software. First-shell fitting was performed in *R*-space in the 1-2.6 Å region for k^2-weighted data Fourier-transformed in the 2-8.2 $Å^{-1}$ *k*-region. Theoretical phases and amplitudes were calculated by Feff 6 code.

2.7. Catalytic Reactions

Generally, 0.75 mL acetic acid (glacial, Fischer), 0.354 mL (2.50 mmol; 10 eq.) 2,6-dimethylanisole (98%, TCI), 36 µL (0.25 mmol; 1 eq.) *n*-butyl acrylate (99+%, Acros), 48 µL (0.25 mmol; 1 eq.) *tert*-butyl peroxybenzoate (TBPB) (98%, Alfa Aesar) and 50 µL hexadecane (internal standard) (>99%, J&K) were added to 40.8 mg (12.5 µmol; 5 mol %) **Pd@TiOP-S1** in a 1.5 mL glass vial. The vials were closed and placed in a preheated 15-well aluminum heating block. The reactions were conducted at 100 °C for 2 hours while stirring. After the reaction, the vials were cooled on ice to quench the reaction and the catalyst was separated from the reaction medium via centrifugation. Product quantification was performed on a Shimadzu GC-2010 with a CP-Sil-5 CB column and a flame ionization detector. Product identification was carried out via GC-MS on an Agilent 6890 gas chromatograph with an HP-1 MS column and a 5973 MSD mass spectrometer.

2.8. Hot filtration test

The reaction was performed under the standard reaction conditions. After 45 min, the reaction was stopped, quickly centrifuged, and the reaction solution was separated from the catalyst powder. The reaction solution was filtered and heated again to 100 °C for the remaining reaction time. Aliquots of 20 µL were taken during the reaction to assess the yield.

2.9. Pd leaching

The leached palladium content in the reaction solution was determined by ICP-OES. After reaction at the standard reaction conditions, the mixture was centrifugated and the reaction solution was separated from the catalyst powder. Next, the organics were evaporated and the remaining metal residue was redissolved in aqua regia. Finally, the aqua regia solution was diluted with a 5% HNO_3 solution and the metal content was analyzed using a Varian 720-ES.

3. RESULTS AND DISCUSSION

3.1. Design and Synthesis of the Metal Oxide Bisphosphonate-based Single-Site Catalysts

Inspired by the bidentate S,O-ligands designed by Fernández-Ibáñez et al.,[32] we synthesized a new thioether ligand with an additional phosphonic acid group (**S1**), which allows for grafting the ligand on a metal oxide support. As supports, bridged titanium oxide-bisphosphonate materials (**TiOP)** were synthesized by a one-step non-hydrolytic sol-gel route (Scheme 1a).[44] These materials were developed only very recently by the group of Mutin and owe their high pore volumes, surface areas, and tunable mesoporosity to the combination of TiO_2 nanodomains held together by rigid aromatic linkers with fully condensed bisphosphonate groups.[44] In the present work, 4,4'-bis(phosphonomethyl)biphenyl (**L1**) was used as a rigid bisphosphonate linker. As shown in Scheme 1b, the **S1** ligands were grafted post-synthetically onto the resulting mesoporous titanium oxide-bisphosphonates and the structural formulas of the functionalized materials were determined from the Ti/P/S ratio measured by energy dispersive X-ray (EDX) spectroscopy and assuming complete condensation (Table S1). After grafting the **S1** ligands, the BET surface area and pore volume decreased from 525 m^2/g to 430 m^2/g and 1.20 cm^3/g to 0.80 cm^3/g, respectively. Neverthe-

Scheme 1. (a) Sol-gel synthesis of the TiOP support in non-aqueous media. (b) Graphical representation of the synthesis steps to transform the TiOP support into the active Pd@TiOP-S1 single-site catalyst.

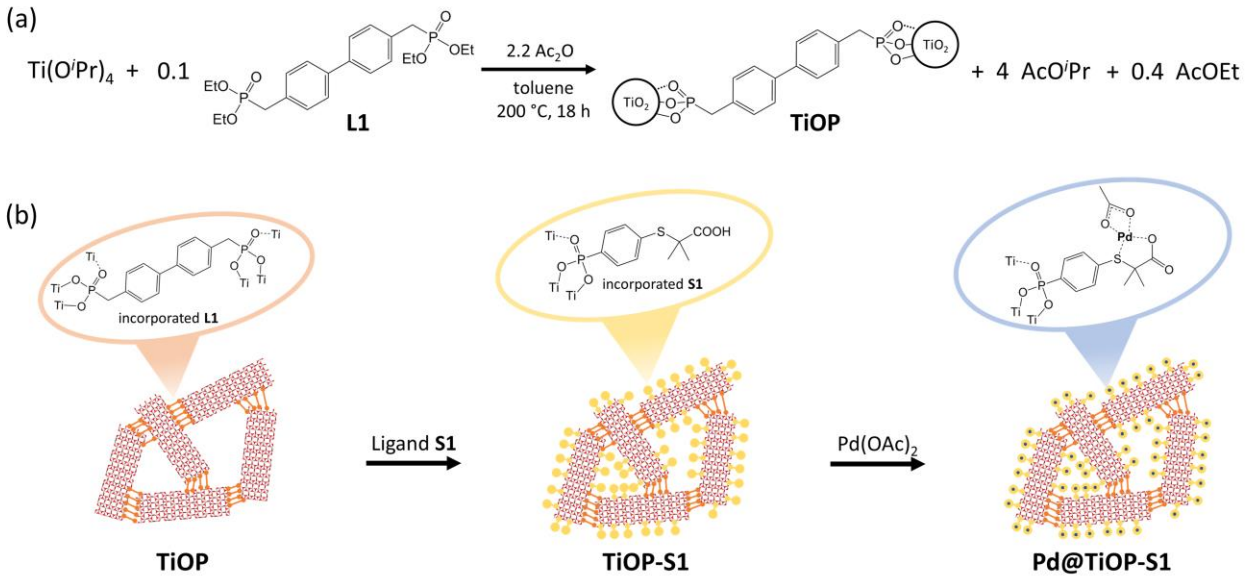

less, the type IV isotherm of the functionalized material confirmed that the grafted support was still mesoporous (Figure 1a). The titanium oxide-bisphosphonate materials were also characterized by solid-state nuclear magnetic resonance (NMR) techniques to gain more information on the structure of the materials. The ^{13}C cross-polarization magic angle spinning (CP-MAS) NMR spectra of **TiOP** and **TiOP-S1** confirm that the bisphosphonate linkers (**L1**) and thioether ligands (**S1**) remain intact after synthesis, while the lack of features around 60 ppm (O-$\underline{C}H_2$-CH3) and 75 ppm (O-$\underline{C}H$-$(CH_3)_2$) implies that the P-OEt and Ti-O^{i}Pr groups, respectively, are fully condensed (Figure 1b). In accordance with the literature, the broad signal centered at 21 ppm in the ^{31}P MAS NMR spectra can be ascribed to the tridentate C-$\underline{P}$-$(OTi)_3$ sites of the bridging bisphosphonate linkers (Figure 1c).[44] Furthermore, an additional signal at 12 ppm can be noted in the spectra of **TiOP-S1** and **TiO_2-S1**, which is ascribed to the tridentate C-$\underline{P}$-$(OTi)_3$ sites of the grafted **S1** ligands (Figure S9).[47] More information on how the **S1** ligands are grafted onto the titanium oxide-bisphosphonate materials was obtained via Fourier-transform infrared (FTIR) spectroscopy (Figure 1d). As for the pure **S1** ligand, a clear carbonyl signal at 1700 cm^{-1} in the spectrum of **TiOP-S1** can be noted, confirming that the **S1** ligand is grafted via its phosphonate group rather than via its carboxylic acid group and that the active S,O-moiety (i.e., a carboxyl group at the α-position of a thioether group) thus remains preserved for Pd(II) anchoring. Finally, analysis of the X-ray diffraction pattern of the **TiOP-S1** material revealed that it consists of anisotropic titanium dioxide anatase nanodomains, which are elongated along the c-axis given the more intense and narrower (004) reflection compared to the (200) reflection (Figure S1). The presence of such anatase nanorods was further evidenced via HR-TEM images, implying that the three-dimensional mesoporous structure of **TiOP-S1** consists of anatase nanorods that are interconnected by the bisphosphonate linkers (Figure S3).

The active **Pd@TiOP-S1** catalyst was obtained by loading the functionalized titanium oxide-bisphosphonate support with $Pd(OAc)_2$. The oxidation state of palladium in the preloaded **Pd@TiOP-S1** catalyst is particularly important since only Pd(II) centers, rather than Pd(0), are catalytically active in oxidative C-H activation reactions. High angle annular dark field scanning transmission electron microscopy (HAADF-STEM) together with energy dispersive X-ray spectroscopy (EDX) indicated that the Pd(II) centers were uniformly distributed over the functionalized titanium oxide-bisphosphonate support (Figure S15). Furthermore, Pd(0) nanoparticles could not be observed in the preloaded material, implying that the active sites of the catalyst are isolated Pd(II) sites. The single-site nature of the preloaded catalyst material was further evidenced by X-ray absorption spectroscopy (XAS). Analysis of the X-ray absorption near edge structure (XANES) revealed that the palladium sites in the preloaded catalyst are present as Pd(II) centers and not as Pd(0) species (Figure S17). In addition, no features resulting from Pd–Pd interactions could be observed in the Fourier transformed extended X-ray absorption fine structure (FT-EXAFS), excluding the presence of Pd(0) nanoparticles and confirming that the palladium centers are dispersed

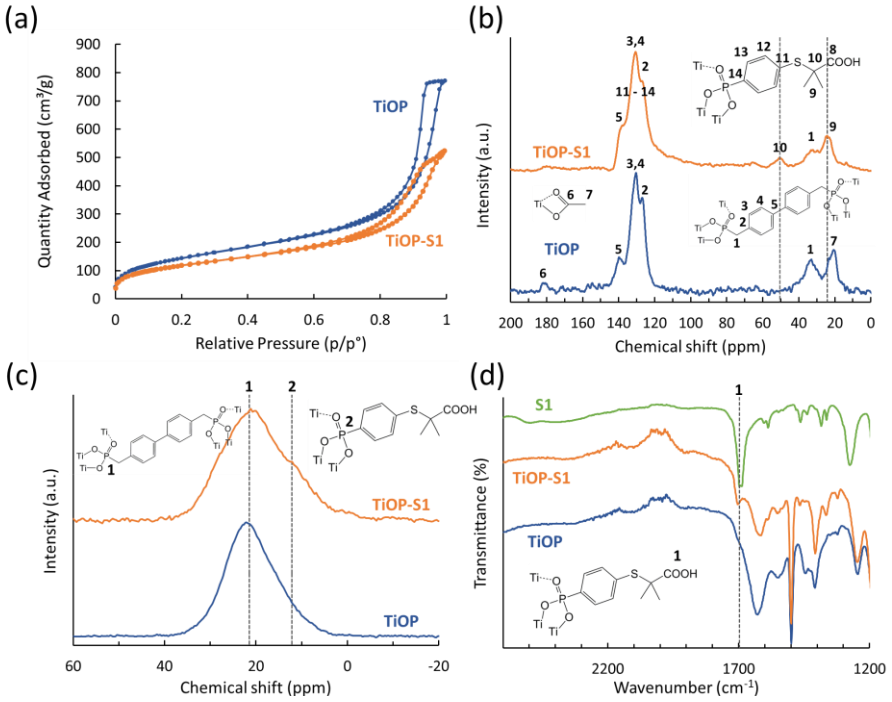

Figure 1. Analysis of the structural properties of **TiOP** (blue) and the functionalized **TiOP-S1** material (orange): (a) N_2 physisorption isotherms, (b) ^{13}C solid-state CP-MAS NMR spectra, (c) ^{31}P solid-state MAS NMR spectra, and (d) FTIR spectra with the reference spectrum of ligand **S1** in green.

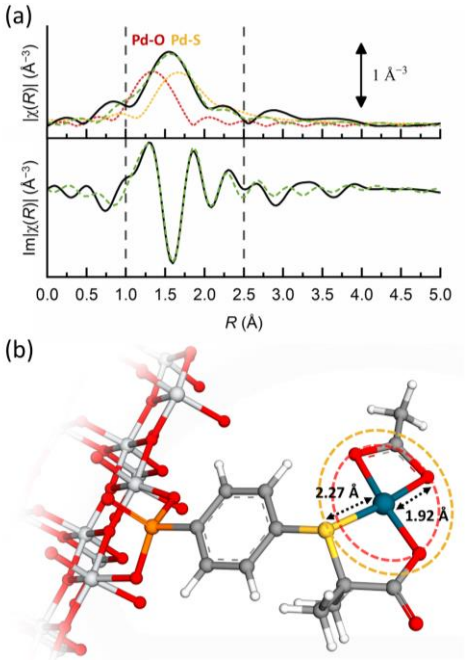

Figure 2. (a) Experimental (solid black line) and best fit (dashed green line) data of the magnitude (top) and imaginary part (bottom) of the Fourier-transformed k^2-weighted EXAFS spectrum of the fresh **Pd@TiOP-S1** catalyst. The Pd-O and Pd-S contributions are shown by red and yellow dotted lines, respectively. (b) Structure model of the Pd(II) active site of **Pd@TiOP-S1** that matches the experimental XAS data. The Ti, P, O, C, H, S, and Pd atoms are displayed as light gray, orange, red, dark gray, white, yellow, and dark blue spheres, respectively. The first and second shell around the Pd(II) center are shown as red and yellow dashed circles, respectively.

over the functionalized titanium oxide-bisphosphonate support as isolated Pd(II) active sites (Figure S18). Furthermore, the structure of the individual Pd(II) active sites could be determined via the FT-EXAFS data. The first shell fitting of the FT-EXAFS data reveals that the Pd(II) centers are surrounded by O- and S-neighbors (Figure 2a) and confirms the proposed structure of **Pd@TiOP-S1** with Pd-O and Pd-S distances of 1.92 ± 0.02 Å and 2.27 ± 0.02 Å, respectively (Figure 2b).

3.2. Catalytic C-H activation reactions

The activity of the obtained **Pd@TiOP-S1** single-site catalyst was tested in the oxidative C-H olefination of arenes, which has been extensively explored in recent years as a more environmentally benign alternative to the widely used traditional Heck cross-coupling reaction.[13,14] After optimizing the reaction conditions (see section 12. of the supporting information), a yield of 75% could be reached employing 5 mol % **Pd@TiOP-S1** as catalyst in the oxidative C-H alkenylation of 2,6-dimethylanisole with *n*-butyl acrylate. This yield was significantly higher than when regular $Pd(OAc)_2$ or Pd(II)-loaded unfunctionalized titanium oxide-bisphosphonate (**Pd@TiOP**) were used as catalyst (Table 1, entries 1-3), confirming that the tailor-made S,O-binding sites of the immobilized **S1** thioether ligands enhance the activity of the Pd(II) centers. When the

Table 1. Comparison of the Activity of the different Catalysts for the Oxidative C-H Alkenylation of 2,6-Dimethylanisole with *n*-Butyl Acrylate[a]

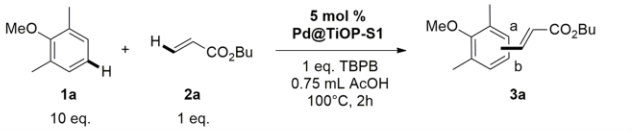

entry	catalyst	yield **3a** (%)[b]	regioselectivity (a:b)
1	$Pd(OAc)_2$	42	1:1.0
2	Pd@TiOP	51	1:1.2
3	Pd@TiOP-S1	75	1.4:1
4	Pd@TiOP-S1[c]	81	1.2:1
5	Pd@TiOP-S1[d]	65	1.4:1
6	$Pd(OAc)_2$ + TiOP-S1	74	1.1:1
7	$Pd(OAc)_2$ + S2	79	1.4:1
8	Pd@TiO_2-S1	43	1.1:1
9	$Pd(OAc)_2$ + TiO_2-S1	41	1.0:1

[a]Reaction conditions: **1a** (2.5 mmol), **2a** (0.25 mmol), **Pd@TiOP-S1** (5 mol % Pd), TBPB (0.25 mmol), and AcOH (0.75 mL) at 100 °C for 2 h. [b]Reaction yield was measured via GC-FID. [c]10 mol % **Pd@TiOP-S1**. [d]2.5 mol % **Pd@TiOP-S1**.

catalyst loading was increased to 10 mol % or decreased to 2.5 mol %, the yield changed accordingly to 81% and 65%, respectively (Table 1, entries 4-5). Furthermore, when $Pd(OAc)_2$ and **TiOP-S1** were added separately, a comparable yield was achieved as with preloaded **Pd@TiOP-S1** (74% vs. 75%, respectively) (Table 1, entries 3 and 6), indicating that the S,O-binding sites of the immobilized **S1** thioether ligands bind the Pd(II) centers with significant affinity and readily combine to form the active **Pd@TiOP-S1** single-site catalyst in situ. Finally, to compare the performance of our heterogeneous catalyst with the state-of-the-art homogeneous system, the original thioether ligand **S2** without phosphonic acid group was added to 5 mol % $Pd(OAc)_2$ under the same reaction conditions. A yield of 79% was obtained (Table 1, entry 7), which is only slightly higher than what is achieved using 5 mol % **Pd@TiOP-S1** (75%).

As a benchmark material for the titanium oxide-bisphosphonate-based catalysts, a mesoporous anatase TiO_2 support was synthesized and subsequently grafted with **S1** ligands (Table S1). After loading **TiO_2-S1** with $Pd(OAc)_2$ in a similar way as **TiOP-S1**, the catalytic performance of the resulting **Pd@TiO_2-S1** material was analyzed. Interestingly, the yield (43%) was considerably lower with 5 mol % **Pd@TiO_2-S1** than when 5 mol % **Pd@TiOP-S1** was used (75%) and only slightly higher than with 5 mol % standard $Pd(OAc)_2$ (Table 1, entry 8). Moreover, even when 5 mol % $Pd(OAc)_2$ and **TiO_2-S1** were added separately (Table 1, entry 9), no significant increase in yield (41%) could be noted. Since the presence of **S1** ligands on the **TiO_2-S1** material was confirmed by EDX,

Table 2. Comparison of the Structure Formula, BET Specific Surface Area (S_{BET}), Total Pore Volume (V_p), Average Pore Diameter (D_p), S1 Loading, and S1 Surface Density of the Functionalized Metal Oxide and Metal Oxide-Bisphosphonate Supports

entry	material	structure formula[a]	S_{BET}[b] (m^2/g)	V_p[c] (cm^3/g)	D_p[d] (nm)	**S1** loading[e] (mmol/g)	**S1** surface density[f] (**S1**/nm^2)
1	TiO_2-S1	$TiO_{1.98}(S1)_{0.02}$	110	0.36	10.6	0.19	1.04
2	TiOP-S1	$TiO_{1.52}(L1)_{0.10}(S1)_{0.04}$	430	0.80	8.7	0.33	0.46
3	TiOP-S1[g]	$TiO_{1.49}(L1)_{0.23}(S1)_{0.05}$	520	0.70	8.7	0.32	0.37
4	Al_2O_3-S1	$Al_2O_{2.92}$ $(S1)_{0.08}$	265	0.46	7.9	0.65	1.48
5	AlOP-S1	$Al_2O_{2.41}(L1)_{0.20}(S1)_{0.19}$	220	0.24	7.2	0.90	2.46
6	ZrO_2-S1	$ZrO_{1.98}(S1)_{0.02}$	80	0.20	5.9	0.15	1.13
7	ZrOP-S1	$ZrO_{1.76}(L1)_{0.08}(S1)_{0.08}$	480	1.05	9.7	0.48	0.59

[a]Structure formulas were determined based on the Ti/P/S EDX ratio assuming complete condensation. [b]BET specific surface area. [c]Total pore volume at $P/P_0 = 0.99$. [d]BJH average pore diameter in the 2-80 nm range calculated from the desorption branch. [e]The **S1** loadings of the supports were determined based on the structure formulas and molecular weights of the bisphosphonate linker **L1** and thioether ligand **S1**. [f]The densities of the **S1** ligands on the surface of the supports were calculated based on the **S1** loadings and BET surface areas. [g]Twice the amount of **L1** added during synthesis.

FTIR, and ^{31}P NMR measurements (Table S1 and Figures S9, and S13), these catalytic results suggest that the grafted **S1** ligands are not well accessible in **TiO_2-S1**. Compared to the mesoporous **TiOP-S1** material, the BET surface area of **TiO_2-S1** is 4 times lower, while the **S1** ligand loading is only 1.7 times lower (Table 2, entries 1-2). As a result, the **S1** surface density is more than two times higher on **TiO_2-S1** (1.04 **S1**/nm^2) compared to **TiOP-S1** (0.46 **S1**/nm^2). Hence, compared to **Pd@TiO_2-S1,** the active S,O-supported Pd(II) sites are more isolated and better accessible on **Pd@TiOP-S1**, resulting in a better single-site catalyst. Additionally, the presence of bisphosphonate linkers with a biphenyl backbone might also increase the affinity of the aromatic substrates towards the active sites on the surface of the supports.

Besides Ti-based materials, functionalized Al and Zr oxide-bisphosphonates and their respective metal oxides were synthesized similarly. EDX, FTIR, and solid-state NMR measurements confirmed that **S1** was incorporated in all materials and that the active S,O-moieties were preserved (Table S1 and Figures S8, and S10-13). After loading with $Pd(OAc)_2$, the obtained catalysts were tested in the oxidative C-H alkenylation reaction to explore the generality of this new catalyst system (Figure 3). While excellent yields could be achieved using **Pd@ZrOP-S1** (73%), the activity of the **Pd@AlOP-S1** catalyst (50%) was considerably lower and only slightly higher than when just $Pd(OAc)_2$ was added (40%). Furthermore, for both metal oxide-based catalysts, **Pd@Al_2O_3-S1** and **Pd@ZrO_2-S1**, the yield was lower than 50%. Again, a clear inverse correlation between the activity and the **S1** surface density of the single-site catalyst could be noted. While **ZrOP-S1** displayed a low **S1** surface density in line with the **TiOP-S1** material, the ligand surface densities on **AlOP-S1**, **Al_2O_3-S1**, and **ZrO_2-S1** materials were all significantly higher (Table 2), confirming that a low **S1** surface density ensures excellent accessibility to the isolated, S,O-supported Pd(II) active sites and ultimately high yields. The remarkably high

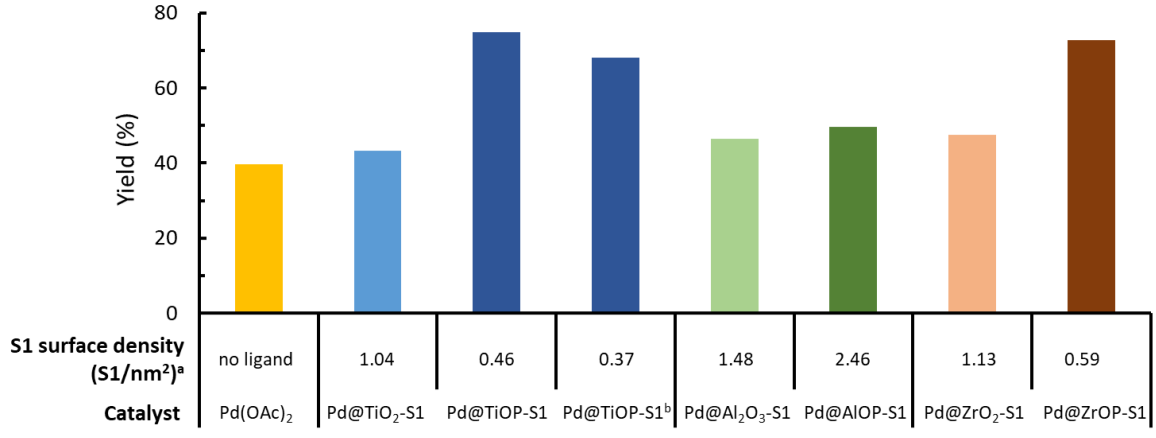

Figure 3. Performance of the different Pd(II)-loaded metal oxide-bisphosphonate catalysts for the oxidative C-H alkenylation of 2,6-dimethylanisole with *n*-butyl acrylate under the standard reaction conditions (cfr. Table 1). [a]The **S1** surface densities were calculated based on the **S1** loadings and BET surface areas (cfr. Table 2). [b]Twice the amount of **L1** added during synthesis (cfr. Table 2).

S1 surface density on **AlOP-S1** is related to the low BET surface area of this support. While the BET surface area of the unfunctionalized **AlOP** material is high (550 m^2/g), it decreases considerably after grafting with **S1** (220 m^2/g) (Table S1), indicating that the support is not stable under the acidic grafting conditions. Furthermore, varying the amount of bisphosphonate linker **L1** in the **TiOP-S1** support did not have a considerable influence on the activity of the corresponding catalyst (Table 2 entry 3 and Figure 3), as long as the **S1** surface density remained low. Adding $Pd(OAc)_2$ and the functionalized supports separately resulted again in similar yields as with preloading (Table S7), reaffirming that the differences in yield are not due to catalyst preparation but rather due to the intrinsic properties of the functionalized materials, such as the surface density of the **S1** ligand. Finally, Pd(II)-loaded Ti-, Al-, and Zr-based oxide-bisphosphonates and metal oxides without **S1** ligands were also tested as control experiments (Table S7). In all cases, only moderate yields were obtained, which further evidences that the presence of isolated, well-accessible **S1** ligands is needed to obtain highly active single-site catalysts.

Having established that the higher yield is due to the isolated, well-accessible S,O-supported Pd(II) centers, the yield was analyzed at several reaction times to determine if this is due to increased catalyst activity or rather to increased catalyst stability (Figure S19). The kinetic profiles clearly show that while all catalysts start to deactivate after 1 hour, already in the initial phase of the reaction, increased yields are achieved with **Pd@TiOP-S1** compared to **Pd@TiOP** or standard $Pd(OAc)_2$, confirming that the tailor-made S,O-binding sites enhance the activity of Pd(II) for the rate-limiting C-H activation step. The slightly higher yield with **Pd@TiOP** compared to $Pd(OAc)_2$, on the other hand, seems to originate from higher catalyst stability, which has been observed before for other porous supports.[41,48] Finally, a TOF of 13 h^{-1} was reached with **Pd@TiOP-S1** after 1 hour, which is among the highest values ever recorded for the non-directed oxidative C-H olefination of arenes.[43]

3.3. Stability of the Catalyst

The stability of the titanium oxide-bisphosphonate support **TiOP-S1** was assessed by comparing the X-ray diffraction patterns of the single-site catalysts before and after the reaction (Figure S1). As expected, no substantial change in the XRD pattern could be noticed, underlining the excellent structural stability of the mesoporous titanium oxide-bisphosphonate supports. Furthermore, nitrogen physisorption measurements showed that the spent **Pd@TiOP-S1** catalyst was still mesoporous. Despite the relatively strong affinity of the tailor-made S,O-binding sites for Pd centers, the presence of Pd(0) nanoparticles in the spent catalyst was evidenced by HAADF-STEM images (Figure S16). This is in line with the kinetic profiles, which show catalyst deactivation after 1 hour. Notably, no sign of aggregation of the sulfur-containing **S1** thioether ligands could be observed, implying that **S1** remained firmly attached to the surface of the titanium oxide-bisphosphonate support during the reaction. Furthermore, inductively coupled plasma optical emission spectrometry (ICP-OES) measurements of the solution after reaction revealed that Pd leaching was minimized to 12 ppm, amounting to a mere 1% leaching. The heterogeneity of the single-site catalyst was also demonstrated by a hot filtration test (Figure S20), highlighting the feasibility of efficient recovery of the expensive Pd centers. Nevertheless, the activity of the single-site catalyst decreased considerably during consecutive runs (Figure S21). Given the minimal Pd leaching and the fact that using an excess of support compared to Pd does not improve the recyclability (Figure S22), this is likely due to the limited catalyst stability. The kinetic profile shows that the catalyst starts to deactivate after 1 hour, presumably due to the formation of Pd(0) aggregates that are apparent in the HAADF-STEM images of the catalyst after reaction and cannot efficiently be reoxidized by TBPB to the active Pd(II) centers. Moreover, no products could be observed in the control reaction with Pd(0) nanopowder (350 – 800 nm nanoparticles) (Table S7), which supports our hypothesis that the poor recyclability is due to Pd(0) nanoparticle formation. Finally, it should be noted that several other Pd-based heterogeneous C-H activation catalyst systems encountered comparable recyclability problems.[42,43]

3.4. Substrate Scope

The substrate scope was explored by testing a broad range of arenes and alkenes (Table 3). The oxidative alkenylation of functionalized arenes containing electron-donating groups furnished the products **3a** – **3d** in excellent yields (81 – 94%). Particularly, 2,6-dimethylphenol was converted in almost quantitative yields (94%), even when only a slight excess of 2,6-dimethylphenol was added, and a TON of 83 could be reached with 1 mol % **Pd@TiOP-S1**. In contrast, the alkenylation products of aromatics bearing alkyl groups (**3e** – **3h)** were obtained in only moderate yields (37 – 54%), and even lower yields (6 – 26%) were obtained using arenes without substituents or with electron-withdrawing substituents (**3i** and **3j**). Since especially arenes with electron-donating groups are efficiently converted by the heterogeneous single-site catalyst, several electron-rich heteroarenes were also tested. While the alkenylation of 2-methylfuran (**3k**) furnished the product in high yield (91%), lower yields were obtained using 2,5-dimethylfuran (**3l**), 2-methylthiophene (**3m**), and 1-methylindole (**3n**) (64%, 40%, and 42%, respectively). Besides *n*-butyl acrylate, methyl acrylate and ethyl acrylate were also tested as olefins, furnishing the products **3o** and **3p**, respectively, in high yields (74 – 77%). Finally, the applicability of our heterogeneous single-site catalyst for the pharmaceutical and specialty chemicals industry was demonstrated by converting industrially relevant reagents. Albeit in moderate regioselectivity for the desired *para*-isomers, excellent yields (81 – 82%) were obtained for products **3q** and **3r**, which are extensively applied as sunscreen ingredients Amiloxate and Octinoxate, respectively.

Table 3. Substrate Scope[a]

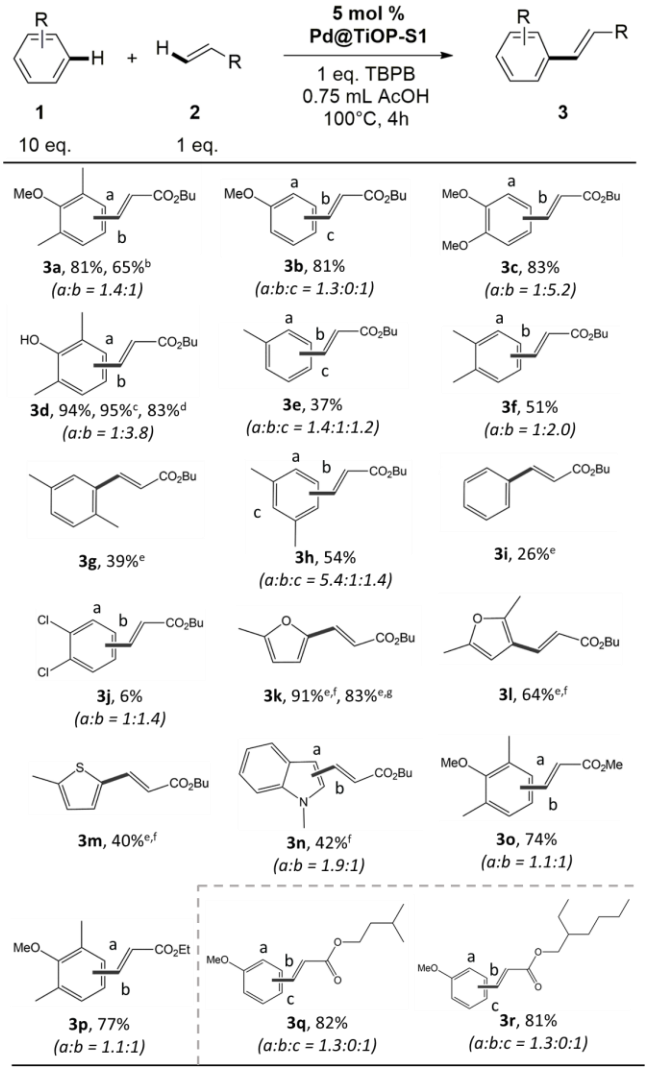

[a]Standard reaction conditions: **1** (2.5 mmol), **2** (0.25 mmol), **Pd@TiOP-S1** (5 mol %), TBPB (0.25 mmol), and AcOH (0.75 mL) at 100 °C for 4 h. Reaction yield was measured via GC-FID and the products were identified via GC-MS. [b]2.5 mol % **Pd@TiOP-S1**. [c]**1** (0.5 mmol). [d]**1** (0.5 mmol), 1 mol % **Pd@TiOP-S1**. [e]Only one regioisomer was formed. [f]**1** (0.5 mmol), 70 °C. [g]**1** (0.5 mmol), 1 mol % **Pd@TiOP-S1**, 70 °C.

4. CONCLUSIONS

In this work, recently developed metal oxide-bisphosphonate materials were grafted with thioether ligands and tested as supports to make Pd(II) single-site catalysts. Based on solid-state ^{13}C and ^{31}P NMR measurements and FTIR spectroscopy, it was established that the thioether ligands were successfully grafted on the metal oxide-bisphosphonate material, while preserving the active S,O-moiety of the ligands for Pd(II)-anchoring. Analysis of the resulting **Pd@TiOP-S1** catalyst via HAADF-STEM, XANES, and FT-EXAFS indicated that the palladium centers were uniformly dispersed as isolated Pd(II) active sites and excluded the presence of Pd(0) nanoparticles in the catalyst before reaction. Moreover, the local environment of the S,O-supported Pd(II) single-sites could be determined via FT-EXAFS. The activity of the obtained **Pd@TiOP-S1** single-site catalyst was tested for the oxidative C-H alkenylation of arenes. A TOF of 13 h^{-1} was achieved with **Pd@TiOP-S1** after 1 h, which was approximately 2-times the TOF reached with standard $Pd(OAc)_2$ and comparable to the activity of state-of-the-art homogeneous systems. Besides the presence of thioether ligands, also textural and surface properties of the support has a major influence on the activity. Significantly more active single-site catalysts were obtained using functionalized, mesoporous metal oxide-bisphosphonates with high specific surface areas and low **S1** surface densities as catalyst support instead of the corresponding functionalized mesoporous metal oxides. This increase in activity seems to be associated with the highly porous nature of the metal-oxide bisphosphonate materials, which could facilitate the presence of isolated, well-accessible S,O-supported Pd(II) active sites. Finally, it was demonstrated that the optimal heterogeneous single-site catalyst furnishes the alkenylation products of several model substrates and industrially relevant arenes in good to excellent yields. However, further progress on the stability and recyclability is still needed to unlock the full potential of this new heterogeneous single-site catalyst for oxidative C-H activation reactions. Nevertheless, this study highlights that the use of such highly porous, organic-inorganic hybrid materials as supports can result in significantly more active single-site catalysts compared to conventional metal oxide supports, which might inspire future research in this rapidly growing domain.

ASSOCIATED CONTENT

Supporting Information. Additional characterization data, optimization of the reaction conditions, and product identification (PDF). This material is available free of charge via the Internet at http://pubs.acs.org.

AUTHOR INFORMATION

Corresponding Authors

* E-mail for D.E.D.V.: dirk.devos@kuleuven.be
* E-mail for P.H.M.: hubert.mutin@univ-montp2.fr

Author Contributions

†These authors contributed equally.

ORCID

Niels Van Velthoven: 0000-0003-3224-0239

Yanhui Wang: 0000-0002-3214-2711

Mickaël Henrion: 0000-0001-8682-5182

Aram Bugaev: 0000-0001-8273-2560

Alexander Soldatov: 0000-0001-8411-0546

Johan Alauzun: 0000-0002-6531-0750

Hubert Mutin: 0000-0002-6031-6467

Dirk De Vos: 0000-0003-0490-9652

Notes

The authors declare no competing financial interest.

ACKNOWLEDGMENTS

This research has received funding from the European Union's Horizon 2020 research and innovation program under grant agreement No. 720996. D. E. D. V. acknowledges the KU Leuven for support via a C3 project and a CASAS Metusalem project. N. V. V. WO for funding (1S32917N). A. L. B. acknowledges the President's Grant of Russian Federation for young scientists MK-2554.2019.2 for financial support of measurement and analysis of XAS data.

REFERENCES

(1) Torborg, C.; Beller, M. Recent Applications of Palladium-Catalyzed Coupling Reactions in the Pharmaceutical, Agrochemical, and Fine Chemical Industries. *Adv. Synth. Catal.* **2009**, *351*, 3027–3043.

(2) Busacca, C. A.; Fandrick, D. R.; Song, J. J.; Senanayake, C. H. The Growing Impact of Catalysis in the Pharmaceutical Industry. *Adv. Synth. Catal.* **2011**, *353*, 1825–1864.

(3) Welch, C. J.; Albaneze-Walker, J.; Leonard, W. R.; Biba, M.; DaSilva, J.; Henderson, D.; Laing, B.; Mathre, D. J.; Spencer, S.; Bu, X.; Wang, T. Adsorbent Screening for Metal Impurity Removal in Pharmaceutical Process Research. *Org. Process Res. Dev.* **2005**, *9*, 198–205.

(4) Colacot, T. J. The 2010 Nobel Prize in Chemistry: Palladium-Catalysed Cross-Coupling. *Platin. Met. Rev.* **2011**, *55*, 84–90.

(5) De Vos, D. E.; Dams, M.; Sels, B. F.; Jacobs, P. A. Ordered Mesoporous and Microporous Molecular Sieves Functionalized with Transition Metal Complexes as Catalysts for Selective Organic Transformations. *Chem. Rev.* **2002**, *102*, 3615–3640.

(6) Thomas, J. M.; Raja, R.; Lewis, D. W. Single-Site Heterogeneous Catalysts. *Angew. Chem., Int. Ed.* **2005**, *44*, 6456–6482.

(7) Copéret, C.; Comas-Vives, A.; Conley, M. P.; Estes, D. P.; Fedorov, A.; Mougel, V.; Nagae, H.; Núnez-Zarur, F.; Zhizhko, P. A. Surface Organometallic and Coordination Chemistry toward Single-Site Heterogeneous Catalysts: Strategies, Methods, Structures, and Activities. *Chem. Rev.* **2016**, *116*, 323–421.

(8) Rogge, S. M. J.; Bavykina, A.; Hajek, J.; Garcia, H.; Olivos-Suarez, A. I.; Sepúlveda-Escribano, A.; Vimont, A.; Clet, G.; Bazin, P.; Kapteijn, F.; Daturi, M.; Ramos-Fernandez, E. V.; Llabrés Xamena, F. X. I.; Van Speybroeck, V.; Gascon, J. Metal-Organic and Covalent Organic Frameworks as Single-Site Catalysts. *Chem. Soc. Rev.* **2017**, *46*, 3134–3184.

(9) Cantillo, D.; Kappe, C. O. Immobilized Transition Metals as Catalysts for Cross-Couplings in Continuous Flow - A Critical Assessment of the Reaction Mechanism and Metal Leaching. *ChemCatChem* **2015**, *6*, 3286–3305.

(10) Hübner, S.; De Vries, J. G.; Farina, V. Why Does Industry Not Use Immobilized Transition Metal Complexes as Catalysts? *Adv. Synth. Catal.* **2016**, *358*, 3–25.

(11) Cui, X.; Li, W.; Ryabchuk, P.; Junge, K.; Beller, M. Bridging Homogeneous and Heterogeneous Catalysis by Heterogeneous Single-Metal-Site Catalysts. *Nat. Catal.* **2018**, *1*, 385–397.

(12) Chen, X.; Engle, K. M.; Wang, D. H.; Jin-Quan, Y. Palladium(II)-Catalyzed C-H Activation/C-C Cross-Coupling Reactions: Versatility and Practicality. *Angew. Chem., Int. Ed.* **2009**, *48*, 5094–5115.

(13) Le Bras, J.; Muzart, J. Intermolecular Dehydrogenative Heck Reactions. *Chem. Rev.* **2011**, *111*, 1170–1214.

(14) Zhou, L.; Lu, W. Towards Ideal Synthesis: Alkenylation of Aryl C-H Bonds by a Fujiwara-Moritani Reaction. *Chem. - Eur. J.* **2014**, *20*, 634–642.

(15) Yang, Y.; Lan, J.; You, J. Oxidative C-H/C-H Coupling Reactions between Two (Hetero)Arenes. *Chem. Rev.* **2017**, *117*, 8787–8863.

(16) Lyons, T. W.; Sanford, M. S. Palladium-Catalyzed Ligand-Directed C-H Functionalization Reactions. *Chem. Rev.* **2010**, *110*, 1147–1169.

(17) Sambiagio, C.; Schönbauer, D.; Blieck, R.; Dao-Huy, T.; Pototschnig, G.; Schaaf, P.; Wiesinger, T.; Zia, M. F.; Wencel-Delord, J.; Besset, T.; Maes, B. U. W.; Schnürch, M. A Comprehensive Overview of Directing Groups Applied in Metal-Catalysed C-H Functionalisation Chemistry. *Chem. Soc. Rev.* **2018**, *47*, 6603–6743.

(18) Engle, K. M.; Yu, J. Q. Developing Ligands for Palladium(II)-Catalyzed C-H Functionalization: Intimate Dialogue between Ligand and Substrate. *J. Org. Chem.* **2013**, *78*, 8927–8955.

(19) Engle, K. M.; Wang, D. H.; Yu, J. Q. Ligand-Accelerated C-H Activation Reactions: Evidence for a Switch of Mechanism. *J. Am. Chem. Soc.* **2010**, *132*, 14137–14151.

(20) Wang, D. H.; Engle, K. M.; Shi, B. F.; Yu, J. Q. Ligand-Enabled Reactivity and Selectivity in a Synthetically Versatile Aryl C-H Olefination. *Science* **2010**, *327*, 315–319.

(21) Zhang, Y.; Shi, B.; Yu, J. Pd(II)-Catalyzed Olefination of Electron-Deficient Arenes Using 2,6-Dialkylpyridine Ligands. *J. Am. Chem. Soc.* **2009**, *131*, 5072–5074.

(22) Kubota, A.; Emmert, M. H.; Sanford, M. S. Pyridine Ligands as Promoters in PdII/0-Catalyzed C-H

Olefination Reactions. *Org. Lett.* **2012**, *14*, 1760–1763.

(23) Chen, H.; Wedi, P.; Meyer, T.; Tavakoli, G.; van Gemmeren, M. Dual Ligand-Enabled Nondirected C–H Olefination of Arenes. *Angew. Chem., Int. Ed.* **2018**, *57*, 2497–2501.

(24) Wang, P.; Farmer, M. E.; Huo, X.; Jain, P.; Shen, P.-X.; Ishoey, M.; Bradner, J. E.; Wisniewski, S. R.; Eastgate, M. D.; Yu, J.-Q. Ligand-Promoted Meta-C–H Arylation of Anilines, Phenols, and Heterocycles. *J. Am. Chem. Soc.* **2016**, *138*, 9269–9276.

(25) Wang, P.; Verma, P.; Xia, G.; Shi, J.; Qiao, J. X.; Tao, S.; Cheng, P. T. W.; Poss, M. A.; Farmer, M. E.; Yeung, K. S.; Yu, J. Q. Ligand-Accelerated Non-Directed C-H Functionalization of Arenes. *Nature* **2017**, *551*, 489–493.

(26) Ye, M.; Gao, G. L.; Yu, J. Q. Ligand-Promoted C-3 Selective C-H Olefination of Pyridines with Pd Catalysts. *J. Am. Chem. Soc.* **2011**, *133*, 6964–6967.

(27) Gao, G. L.; Xia, W.; Jain, P.; Yu, J. Q. Pd(II)-Catalyzed C3-Selective Arylation of Pyridine with (Hetero)Arenes. *Org. Lett.* **2016**, *18*, 744–747.

(28) Campbell, A. N.; Meyer, E. B.; Stahl, S. S. Regiocontrolled Aerobic Oxidative Coupling of Indoles and Benzene Using Pd Catalysts with 4,5-Diazafluorene Ligands. *Chem. Commun.* **2011**, *47*, 10257–10259.

(29) Vasseur, A.; Laugel, C.; Harakat, D.; Muzart, J.; Bras, J. Le. Ligand-Promoted Reactivity of Alkenes in Dehydrogenative Heck Reactions of Furans and Thiophenes. *Eur. J. Org. Chem.* **2015**, *2015*, 944–948.

(30) Gorsline, B. J.; Wang, L.; Ren, P.; Carrow, B. P. C-H Alkenylation of Heteroarenes: Mechanism, Rate, and Selectivity Changes Enabled by Thioether Ligands. *J. Am. Chem. Soc.* **2017**, *139*, 9605–9614.

(31) Wang, L.; Carrow, B. P. Oligothiophene Synthesis by a General C-H Activation Mechanism: Electrophilic Concerted Metalation-Deprotonation (ECMD). *ACS Catal.* **2019**, *9*, 6821–6836.

(32) Naksomboon, K.; Valderas, C.; Gómez-Martínez, M.; Álvarez-Casao, Y.; Fernández-Ibáñez, M. Á. S,O-Ligand-Promoted Palladium-Catalyzed C–H Functionalization Reactions of Nondirected Arenes. *ACS Catal.* **2017**, *7*, 6342–6346.

(33) Naksomboon, K.; Álvarez-Casao, Y.; Uiterweerd, M.; Westerveld, N.; Maciá, B.; Fernández-Ibáñez, M. Á. S,O-Ligand-Promoted Palladium-Catalyzed C–H Olefination of Arenes with Allylic Substrates. *Tetrahedron Lett.* **2018**, *59*, 379–382.

(34) Naksomboon, K.; Poater, J.; Bickelhaupt, F. M.; Fernández-Ibáñez, M. Á. Para-Selective C–H Olefination of Aniline Derivatives via Pd/S,O-Ligand Catalysis. *J. Am. Chem. Soc.* **2019**, *141*, 6719–6725.

(35) Álvarez-Casao, Y.; Fernández-Ibáñez, M. Á. S,O-Ligand-Promoted Pd-Catalyzed C–H Olefination of Thiophenes. *Eur. J. Org. Chem.* **2019**, *2019*, 1842–1845.

(36) Hayler, J. D.; Leahy, D. K.; Simmons, E. M. A Pharmaceutical Industry Perspective on Sustainable Metal Catalysis. *Organometallics* **2019**, *38*, 36–46.

(37) Santoro, S.; Kozhushkov, S. I.; Ackermann, L.; Vaccaro, L. Heterogeneous Catalytic Approaches in C-H Activation Reactions. *Green Chem.* **2016**, *18*, 3471–3493.

(38) Dhakshinamoorthy, A.; Asiri, A. M.; Garcia, H. Formation of C-C and C-Heteroatom Bonds by C-H Activation by Metal Organic Frameworks as Catalysts or Supports. *ACS Catal.* **2019**, *9*, 1081–1102.

(39) Duan, H.; Li, M.; Zhang, G.; Gallagher, J. R.; Huang, Z.; Sun, Y.; Luo, Z.; Chen, H.; Miller, J. T.; Zou, R.; Lei, A.; Zhao, Y. Single-Site Palladium(II) Catalyst for Oxidative Heck Reaction: Catalytic Performance and Kinetic Investigations. *ACS Catal.* **2015**, *5*, 3752–3759.

(40) Zhang, W.; Asakura, H.; Qin, Q.; Wang, J.; Li, J.; Yan, N.; Zhou, Y.; Wang, Q.; Liu, Y. Direct Aerobic Oxidative Homocoupling of Benzene to Biphenyl over Functional Porous Organic Polymer Supported Atomically Dispersed Palladium Catalyst. *Appl. Catal. B Environ.* **2017**, *209*, 679–688.

(41) Van Velthoven, N.; Waitschat, S.; Chavan, S. M.; Liu, P.; Smolders, S.; Vercammen, J.; Bueken, B.; Bals, S.; Lillerud, K. P.; Stock, N.; De Vos, D. E. Single-Site Metal–Organic Framework Catalysts for the Oxidative Coupling of Arenes via C–H/C–H Activation. *Chem. Sci.* **2019**, *10*, 3616–3622.

(42) Otake, K.; Ye, J.; Mandal, M.; Islamoglu, T.; Buru, C. T.; Hupp, J. T.; Delferro, M.; Truhlar, D. G.; Cramer, C. J.; Farha, O. K. Enhanced Activity of Heterogeneous Pd(II) Catalysts on Acid-Functionalized Metal–Organic Frameworks. *ACS Catal.* **2019**, *9*, 5383–5390.

(43) Van Velthoven, N.; Henrion, M.; Dallenes, J.; Krajnc, A.; Bugaev, A. L.; Liu, P.; Bals, S.; Soldatov, A. V.; Mali, G.; De Vos, D. E. S,O-Functionalized Metal–Organic Frameworks as Heterogeneous Single-Site Catalysts for the Oxidative Alkenylation of Arenes via C–H Activation. *ACS Catal.* **2020**, *10*, 5077–5085.

(44) Wang, Y.; Alauzun, J. G.; Mutin, P. H. Water-Stable, Nonsiliceous Hybrid Materials with Tunable Porosity and Functionality: Bridged Titania-Bisphosphonates. *Chem. Mater.* **2020**, *32*, 2910–2918.

(45) Wang, Y.; Kim, S.; Louvain, N.; Alauzun, J. G.; Mutin, P. H. Acetic Anhydride as an Oxygen Donor in the Non-Hydrolytic Sol–Gel Synthesis of Mesoporous TiO 2 with High Electrochemical Lithium Storage Performances. *Chem. - Eur. J.* **2019**, *25*, 4767–4774.

(46) Acosta, S.; Corriu, R. J. P.; Leclercq, D.; Lefèvre, P.; Mutin, P. H.; Vioux, A. Preparation of Alumina Gels by a Non-Hydrolytic Sol-Gel Processing Method. *J. Non. Cryst. Solids* **1994**, *170*, 234–242.

(47) Brodard-Severac, F.; Guerrero, G.; Maquet, J.; Florian, P.; Gervais, C.; Mutin, P. H. High-Field 17O MAS NMR Investigation of Phosphonic Acid Monolayers on Titania. *Chem. Mater.* **2008**, *20*, 5191–5196.

(48) Anastasiou, I.; Van Velthoven, N.; Tomarelli, E.; Lombi, A.; Lanari, D.; Liu, P.; Bals, S.; De Vos, D. E.; Vaccaro, L. C2–H Arylation of Indoles Catalyzed by Palladium-Containing Metal-Organic-Framework in γ-Valerolactone. *ChemSusChem* **2020**, *13*, 1–7.